Bull. Mater. Sci. (2021)44:55
https://doi.org/10.1007/s12034-020-02338-6

Bulk growth of Iminodiacetic acid single crystal and its characterization for nonlinear optical applications

DEBABRATA NAYAK[1,2], N VIJAYAN[1,2,*], MANJU KUMARI[1,2], MAHAK VIJ[1,2], B SRIDHAR[3], GOVIND GUPTA[1,2] and R P PANT[1,2]

[1] Academy of Scientific and Innovative Research, CSIR – Human Resource Development Centre, (CSIR–HRDC) Campus, Ghaziabad 201002, India
[2] CSIR – National Physical Laboratory, New Delhi 110012, India
[3] CSIR – Indian Institute of Chemical Technology, Hyderabad 500007, India
*Author for correspondence (nvijayan@nplindia.org; vjnphy@gmail.com)

MS received 24 July 2020; accepted 30 September 2020

Abstract. A bulk size transparent nonlinear organic single crystal of Iminodiacetic acid was harvested using slow evaporation solution growth technique in controlled atmosphere with a span of 4 weeks. The structural properties of titled crystal were examined by single-crystal X-ray diffraction. The quality of the ingot was determined by high-resolution X-ray diffraction and found that the sample is free from grain boundaries. From UV–Vis analysis, one can understand that there is less absorption in the entire wavelength range of visible region and observed cut-off wavelength is 242 nm. From photoluminescence analysis, the emission of wavelength is identified at 421 nm. Mechanical strength and various parameters like work-hardening coefficient and stiffness constant of ingot was measured using Vickers microhardness test and corresponding experimental data had been explained using distinct theoretical models. The variation measurement of dielectric constant and dielectric loss in respect of frequency was carried out to compute the electronic polarizability of titled compound using Penn model. The detailed analysis of third-harmonic generation was executed using Z-scan method. The values of nonlinear refractive index (n_2) and two photon absorption coefficient (β) were obtained to be 2.19×10^{-17} cm^2 W^{-1} and 4.25×10^{-12} cm W^{-1}, respectively. The higher value of coupling factor suggests nonlinear absorption is more dominant and the crystal is suitable for optical limiting application.

Keywords. Crystal growth; X-ray analysis; mechanical; nonlinear optics; dielectric; Z-scan.

1. Introduction

The current science and technology requires potential nonlinear optical (NLO) single crystals for their varieties of applications in different fields, such as optical limiting, lasers, fibre optics communication, optical data storage, etc. The above said efficient materials can be grown using different techniques [1,2]. Generally, organic crystals are more optically nonlinear than inorganic, because of its hydrogen as well as Vander Waal's bonds and also high degree of delocalization of electrons. It is also found that organic molecules possess high laser damage threshold (LDT) with wide range of optical bandgap and good thermal stability, which make them suitable for fabrication of various devices [3,4]. Iminodiacetic acid (IMDA) is an acid amine having lone pair at nitrogen connected to two CH_2 groups, which are bonded with carboxylic group. The title compound was first reported by Tomita *et al* [5] and observed that this material crystallizes in three different forms of phases, such as α, β and γ. The present compound of IMDA belongs to 'α' form and crystallizes in noncentrosymmetric in nature and shows various NLO properties. The presence of nitrogen atoms and carboxylic groups in IMDA act as ligand to form a metal complex, which can be used for removal of metal ion from industrial waste solution. The harvested crystal also shows the NLO applications like second-harmonic generation (SHG), which signifies the usefulness of titled material [5,6].

In the current investigation, we are reporting the growth of bulk size IMDA single crystal by slow evaporation solution growth technique (SEST) and studied its various properties for NLO applications. Especially third-order nonlinearity of IMDA crystal has been studied using Z-scan technique to find its suitability in NLO, optoelectronic and device applications. To the best of our knowledge, there is no such report which defines the third-order NLO behaviour of the grown crystal except SHG behaviour of the same by Tomita *et al* [5]. This is the first article that consists of detailed mechanical analyses and Z-scan measurements, which are mandatory for machining novel NLO devices.

Published online: 04 March 2021

Figure 1. Photograph of IMDA crystal.

Table 1. Crystallographic data.

Unit cell parameters	Reported	Experimental
a	5.267 Å	5.262 Å
b	14.140 Å	14.150 Å
c	14.933 Å	14.916 Å
Crystal system	Orthorhombic	Orthorhombic

2. Crystal growth

The commercially available material (purity: 99%) was used as the source material for growing the title compound. Its purity was improved by frequent recrystallization. A saturated mother solution of IMDA was made by dissolving the solute in deionized water by continuous stirring for 4 h. After preparing the concentrated solution, filtration was performed using a Whatman filter paper and covered by thin plastic cover. Then it was housed in a constant temperature bath (CTB) maintained at temperature of 36°C (with accuracy ±0.5°C). The nucleation was started after few days and the bulk size (47 mm × 9 mm × 6 mm) of single crystal was harvested from the mother solution after a time period of a month. The mentioned bulk crystal is presented in figure 1.

3. Results and discussion

3.1 *X-ray diffraction analysis*

The structural information and lattice dimensions of grown IMDA single crystal was determined using a single-crystal X-ray diffractometer (Model: Bruker D8 QUEST) with IμS microsource (wavelength (λ) = 0.7107 Å) at atmospheric temperature. From this investigation, it was noticed that the grown ingot corresponds to orthorhombic structure and crystallizes in noncentrosymmetric having space group $Pbc2_1$. The calculated unit cell parameters are good acceptance with the literature [5]. The calculated lattice dimensions are given in table 1. From the table, one can understand that the deviation in the calculated one with the reported may be due to the presence of strain in the sample. The observed powder X-ray diffraction (PXRD) pattern of mentioned crystal is given in figure 2. The strain was calculated using Willamson–Hall (W–H) relation [7]

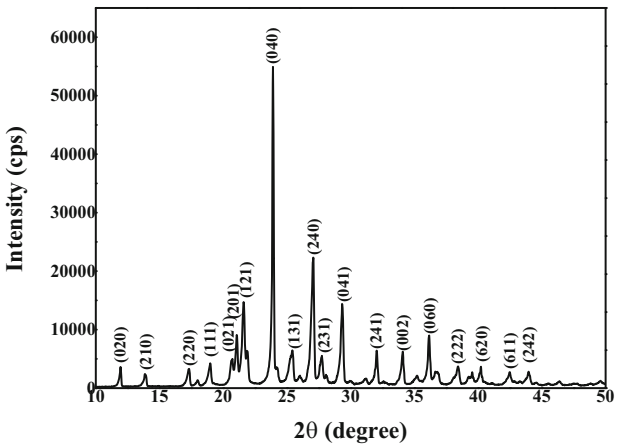

Figure 2. PXRD pattern.

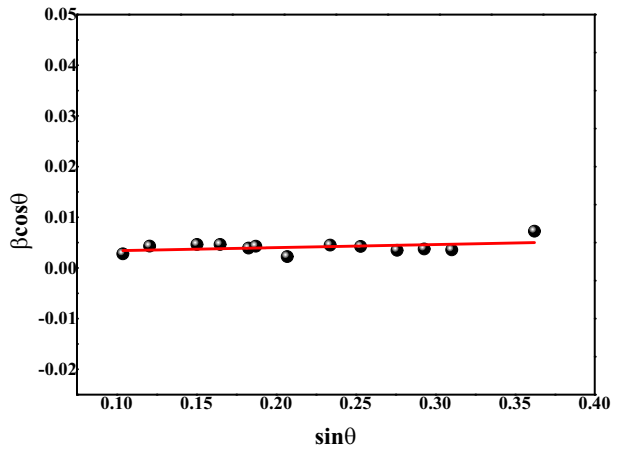

Figure 3. W–H plot.

$$\beta \cos\theta = \frac{K\lambda}{D} + \eta \sin\theta, \quad (1)$$

where β, D, η and K are the full-width half-maxima (FWHM), crystallite size, strain present and the Scherrer constant, respectively. A graph between $\beta \cos\theta$ and $\sin\theta$ was plotted as shown in figure 3, where slope gave the strain in the crystal which was found to be 0.006. The crystallite size had been calculated using intercept of given graph. The average crystallite size was obtained to be 0.046 μm.

3.2 *High-resolution x-ray diffraction*

The crystalline perfection of IMDA single crystal was investigated by recording the diffraction curve (DC) using

high-resolution X-ray diffraction (HRXRD). A well-polished ingot with (040) planes was employed to a PANalytical X'Pert PRO MRD high-resolution X-ray diffractometer system and recorded DC is shown in figure 4. The single peak in DC implies that the sample is free from grain boundaries. The FWHM of the intense peak is 33 arc sec, which is higher than the value obtained from the plane wave theory of dynamical XRD for an ideally perfect crystal, but reasonably nearby the value expected for perfect crystals [8]. The symmetry of DC can be identified by setting Bragg's diffraction peak position to zero and the asymmetry with good scattered intensity was found in the positive side of DC, which points out that IMDA crystal contains interstitial type of defects that are dominating more than vacancy defects. However, concentration of such defects is lesser which eventually affects the performance of devices built on such ingot single crystals.

3.3 *UV–Visible spectroscopy*

It is very much important that a crystal to be transparent in wide range of light spectra for practical applications in nonlinear optics. The optical properties provide the information about electronic band structure and types of optical transition occurring in solids [9]. The optical transmittance of the as-grown IMDA crystal of thickness 3 mm was taken for the present case and spectra was recorded between 200 and 1100 nm, and it is shown in figure 5. It was found that the crystal had good transmittance in complete visible region with a UV cutoff wavelength (λ) of 242 nm. The lower UV cutoff may be explained by the appearance of chromophores like amino and carboxylic groups that made the crystal transparent and results almost no absorption in the UV region. The lower UV cutoff also suggests about gradual and consistent degradation of transmittance in near-UV region, as all the incident photons are excited to the higher nonbonding energy states [10].

In order to evaluate optical bandgap relation of absorption coefficient (α), photon energy ($h\upsilon$) was taken into consideration and absorption coefficient (α) can be written by following equation [11]:

$$\alpha = \frac{1}{t}\log\left(\frac{1}{T}\right) \tag{2}$$

Here T denotes transmittance and t the thickness of used ingot accordingly. The absorption coefficient of grown direct bandgap single crystal is related with photon energy as follows [12]:

$$(\alpha h\upsilon)^2 = A\left(E_g - h\upsilon\right) \tag{3}$$

$h\upsilon$ being the energy of photon and E_g represents optical bandgap. The details of the bandgap study have been given in figure 6 and it was obtained to be 4.91 eV.

The wide bandgap and higher value of transmittance of the specimen makes it suitable for application in conversion of infrared light to visible light and in the generation of higher harmonics in the field of laser applications [13].

3.4 *Photoluminescence*

Photoluminescence analysis is an advantageous nondestructive technique for identifying the fluorescence

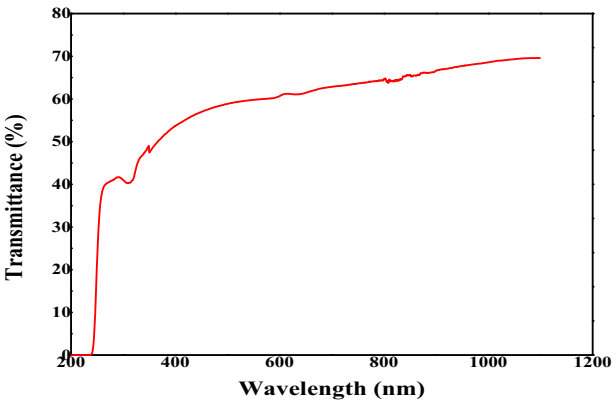

Figure 5. Transmittance *vs.* wavelength.

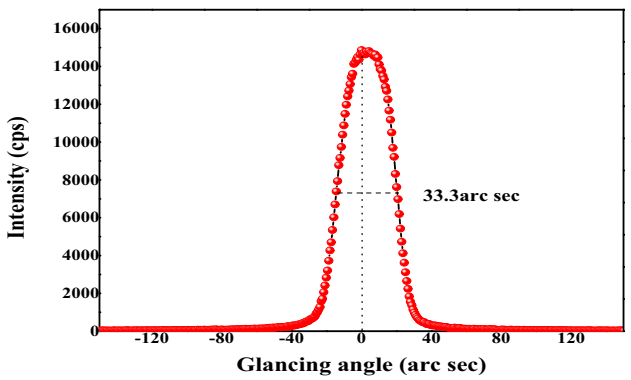

Figure 4. HRXRD pattern.

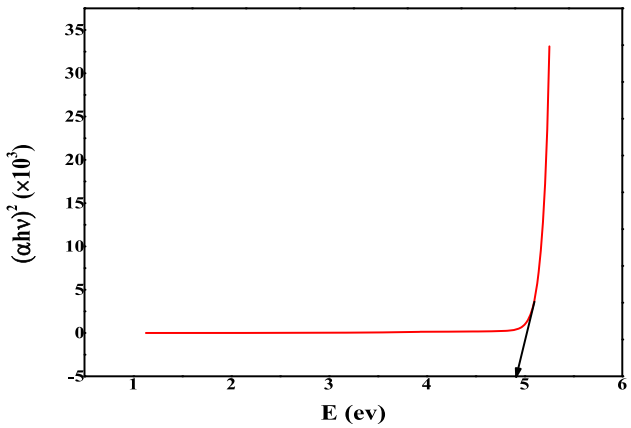

Figure 6. Tauc's plot.

behaviour and electronic structure of the materials. In addition to these properties, crystal quality, impurities, defects and dislocations present in the harvested crystal can also be analysed by using this tool [14]. The grown single crystal was excited with a wavelength of 368 nm using a Xenon (Xe) flash lamp as a source at ambient temperature and the corresponding emission peak at 421 nm was obtained, which is given in figure 7. In the spectrum, there is a sharp single emission peak of energy 2.95 eV, which suggests that there is no impurity and the crystal has minimum defects. It may be concluded that the emission peak is due to the occurrence of electron donating group OH and accepting group C=O. The band separation obtained from PL is lesser than the bandgap obtained from UV–Visible spectroscopy, this arises due to the radiative transition of trapped electrons and trapped holes from the localized state situated between the bandgaps.

3.5 *Mechanical stability analysis*

To understand the mechanical behaviour of the harvested single crystal, the cut and polished specimen was taken and underwent for Vickers microhardness analysis. For device fabrications, it is much important to have knowledge about the mechanical strength of that particular material. For the study of mechanical strength, elastic-plastic behaviour of the harvested single crystal, Vickers microhardness experiment was performed with pyramidal diamond indenter at room temperature. A wide range of load from 5 to 100 g were indented on the surface of solution-grown sample, free from cracks for dwell time of 10 s. For each load, minimum five indentations were taken and the corresponding hardness was recorded. The recorded hardness (H_v) plot is shown in figure 8 and was observed that in low load range H_v increases with the increment of load. This rise in hardness for low load range (below 50 g) was due to piercing of intender on the top of the surface revealing that crystal possess reverse indentation size effect (RISE). For further increment of load, it was observed that H_v was load independent, i.e., it became saturated. The saturation in the hardness was due to the rearrangement of dislocation, which in return increases the mutual interaction stresses [15].

Now some theoretical studies have been performed to explain phenomena like RISE and get to know about the mechanical behaviour of the material. According to Meyer's law for indentation size effect (ISE)

$$P = Kd^n \tag{4}$$

Here n is known as Meyer's index or work hardening, this value explains ISE behaviour in the material and also distinguish between the materials either being soft or hard. For material having n value less than 2 shows normal ISE, which means decrease in hardness with rise in applied load. If $n = 2$, then hardness is load independent, whereas if $n > 2$, RISE is observed that corresponds to increase in H_v with the increase in load [16]. To demonstrate RISE in case of single crystal of IMDA, a graph of log P *vs.* log d is plotted in figure 9, where slope of linearly fitted curve determined the value of n, which was achieved to be 2.413. It shows that material used for study comes under soft category [17]. The average hardness for above material was evaluated using

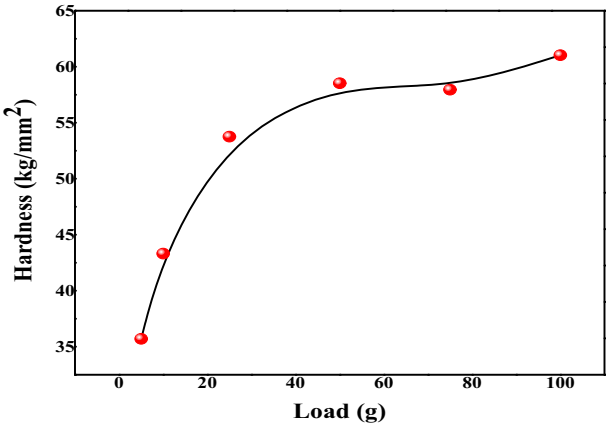

Figure 8. Hardness *vs.* load.

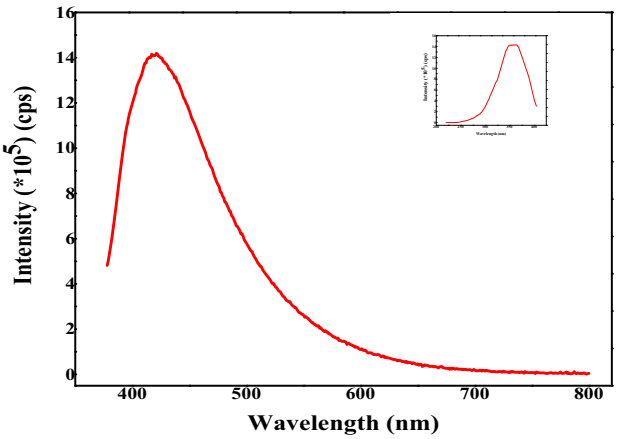

Figure 7. Photoluminescence spectra.

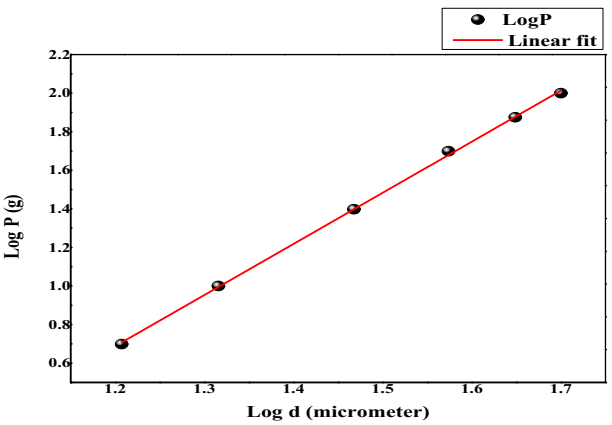

Figure 9. Log P *vs.* log d.

the formula $H_v = 1854.4P/d^2$ and by Meyer's formula that shows both the results are nearly equal.

In order to find out the resistance pressure that can be defined as the minimum load to initiate plastic deformation, Hay–Kendall's law had been taken in account [18]. The expression for the dependence of indentation size on applied load may be given by:

$$P = W + Cd^2 \tag{5}$$

where W represents resistance pressure and C the constant independent of load. The value of W was calculated from the plot between P and d^2, where W was found to have negative value that could predict the material exhibit reverse ISE as shown in figure 10 [19]. The load independent hardness is also calculated from the above plot, which is given by $H_0 = 1854.4$ Ckg mm^{-2}. The values of the above quantities are represented in table 2.

According to proportional specimen model (PSR), load P can be expressed as a function of indentation size represented in equation (6):

$$P = Ad + Bd^2 \tag{6}$$

In this expression, A is related to load-dependent hardness and B corresponds to load-independent hardness. A plot of P/d *vs.* d is given in figure 11, in which slope is used to obtain the minimum hardness (H_{0p}), after which it will become load independent [20].

The average value of hardness from Mayer's formula, the hardness from Hay–Kendall's model and PSR model is given in table 2. The average value of stiffness constant was found using Wooster formula $C_{11} = H_v^{7/4}$ and was calculated to be 0.978×10^5 MPa, which was very large. The obtained result of C_{11} gives the idea that the tightness of the bonds among ions in IMDA was very strong and hence the material had good mechanical properties [21].

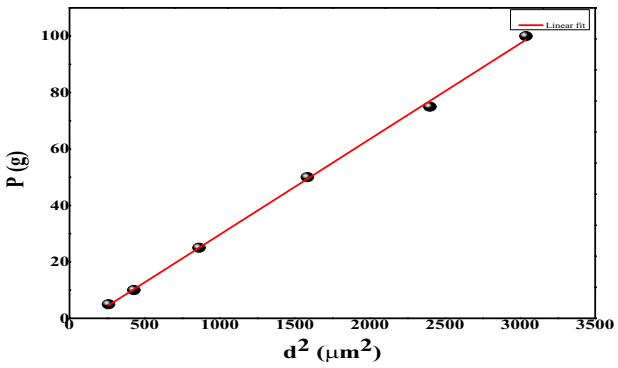

Figure 10. *P vs.* d^2.

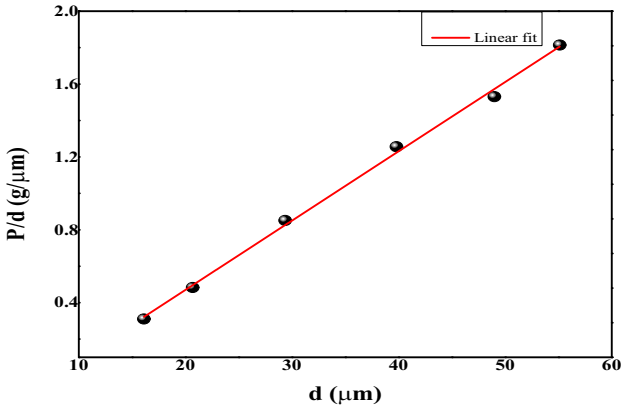

Figure 11. *P/d vs. d.*

3.6 *Dielectric studies*

Dielectric measurement for NLO single crystal is very much effective for getting information about molecular anisotropy, structural changes, electro-optical molecular responses, and transport phenomena within the crystalline material [22–24]. The low dielectric constant material can be useful for faster application and better performance of microelectronics devices. Its utilization can significantly minimize the RC time delay and power dissipation in new generation of high-speed circuit [25]. Predominantly this analysis gives the information about dielectric constant, which depends on parameters like extrinsic nature of material, electronic, space charge, ion and oriental polarizations, respectively [26]. In order to study dielectric constant and loss of the crystal for a variation of frequency (F) at room temperature, a polished sample having dimensions 6.85 mm × 3 mm × 1.89 mm was taken and pasted with conducting silver for making smooth electrical contact. Then sample was placed in a thermal insulated chamber in order to restrict the thermal fluctuations. Then an alternating current (AC), electrical signal of frequency ranging from 100 Hz to 1 MHz was applied between the two electrodes and the variation of

Table 2. Mechanical studies.

Experimental results	Mayer's law	Hay–Kendall's law	PSR model	C_{11}
Average $H_v = 48.366$ kg mm^{-2}	Average $H_v = 51.604$ kg mm^{-2} $n = 2.413$	$H_0 = 62.79$ kg mm^{-2} $W = -4.2181$	$H_{0p} = 70.54$ kg mm^{-2}	0.978×10^5 Mpa

capacitance with frequency was observed. The dielectric constant (ε_∞) was determined by:

$$\varepsilon_\infty = \frac{Cd}{A\varepsilon_0} \tag{7}$$

C, A, d, ε_0 are the capacitance, area, thickness and permittivity of material correspondingly. It was perceived from the plot shown in figure 12 that the ε_∞ decreases exponentially with increase in frequency and became almost constant for higher range of frequencies. Higher value of ε_∞ at lower frequencies is due to the existence of ionic, space, oriental and electronic polarizations. As the frequency increases these polarizations lose their effectiveness, resulting in lower values of dielectric constant [27]. As seen in figure 13, the dielectric loss for higher frequencies was low, which suggested that IMDA crystal possessed enriched optical quality with less defects. This behaviour of the material signifies the suitability of IMDA crystal for opto-electronic applications and NLO device fabrication [28].

Further electronic polarizability had been evaluated using Clausius–Mossotti relation and compared with the theoretical calculation, which was done using Penn model. This is also compared with the electronic polarizability determined from bandgap, which was determined from UV–Vis analysis. The detailed study is given below.

3.6a *Electronic properties of IMDA single crystal:* The electronic properties of the above sample had been determined using the dielectric constant (ε_∞) at higher frequencies. For higher frequency, dielectric constant depends on number of valence electrons, which is related to Plasmon energy and Penn energy explicitly. Penn energy is defined as the average energy related to dielectric constant at higher frequencies, which depends on Plasmon energy [29]. In this work, electron polarizability of the material has been calculated with the help of theoretical model given by Penn using the experimental dielectric constant at high frequencies. Further, it has been calculated using Clausius–Mossotti relation and by using optical bandgap. In addition to electrical polarizability many

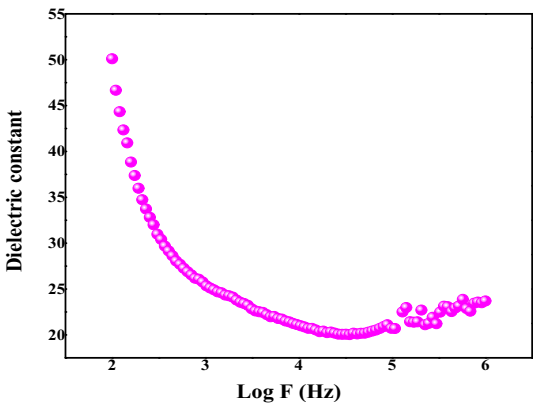

Figure 12. Variation of dielectric constant with frequency.

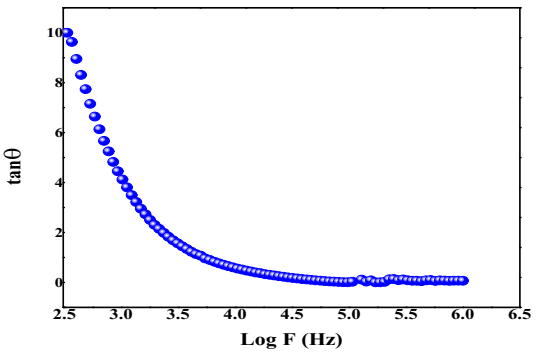

Figure 13. Dielectric loss with frequency.

other electronic parameters like Fermi energy, Penn gap energy and Plasmon energy were reported in the current work. The Plasmon energy ($\hbar\omega_p$) can be calculated using equation (8):

$$\hbar\omega_p = 28.8\left[\frac{Z\rho}{M}\right]^{(1/2)}\text{eV} \tag{8}$$

Z represents sum of the total number of outer most shell electrons for each atom in the molecule, density ρ is in g cm^{-3} and M is molecular mass for the material. The Plasmon energy was computed to be 22.77 eV. Applying Penn model, the average energy gap (E_p) for the single crystal of IMDA is given by [30]:

$$E_p = \frac{\hbar\omega_p}{[\varepsilon_\infty - 1]^{1/2}}\text{eV} \tag{9}$$

where ε_∞ = 23.61 is the dielectric constant at higher frequencies, now the Fermi energy of the titled sample is represented by:

$$E_F = 0.2948\left(\hbar\omega_p\right)^{(4/3)}\text{eV} \tag{10}$$

The electronic polarizability of single crystal is given by the expression:

$$\alpha = \left[\frac{\left(\hbar\omega_p\right)^2 S_0}{\left(\hbar\omega_p\right)^2 S_0 + 3E_p^2}\right] \times \frac{M}{\rho} \times 0.396 \times 10^{-24}\,\text{cm}^3 \tag{11}$$

where S_0 is material constant and can be calculated using:

$$S_0 = 1 - \frac{E_p}{4E_F} + \frac{1}{3}\left[\frac{E_p}{4E_F}\right]^2 \tag{12}$$

Now electronic polarization is determined using Clausius–Mossotti relation:

$$\alpha = \left[\frac{3M}{4\pi N_a \rho}\right]\left[\frac{\varepsilon_\infty - 1}{\varepsilon_\infty + 2}\right] \tag{13}$$

It has been seen that the value for electron polarizability obtained from equation (11) nearly matched with the value determined from Clausius–Mossotti relation. Considering

Table 3. Dielectric studies.

Different parameters	Values
Plasmon energy	22.77 eV
Penn energy	4.789 eV
Fermi energy	19.026 eV
Electron polarizability (α) from Penn approximation	2.886×10^{-23} cm^3
S_0 material constant	0.9384
α from Clausius–Mossotti	2.911×10^{-23} cm^3
α from optical bandgap	1.496×10^{-23} cm^3

the polarizability has a dependence on optical bandgap, the value of α can be determined as follows:

$$\alpha = \left[1 - \frac{\sqrt{E_g}}{4.06}\right] \times \frac{M}{\rho} \times 0.396 \times 10^{-24}\,\text{cm}^3 \tag{14}$$

The value obtained using this formula was also found to be nearly equal to the values determined from previous equations (11 and 13). The electronic parameters values that were calculated from above analysis are given in table 3.

3.7 *Third-order NLO study*

Z-scan technique had been widely adopted to study the third-order nonlinearity in the sample. For the determination of nonlinear absorption (NLA) coefficient (β) and nonlinear refractive (NLR) index (n_2), open aperture and closed aperture Z-scan experiment was performed [31]. The magnitude and sign of the above parameters were evaluated using the corresponding experimental data in order to find out the nature of the sample. For the measurement, Gaussian laser beam of wavelength (λ_L) 800 nm of femto second laser with peak intensity (I_0) 2.2×10^{12} W cm^{-2} was made to focus by a convex lens of focal length (f) 40 cm on the used crystal of having thickness (L) 0.3 cm. Due to the high intensity, the laser beam induces nonlinearity in the crystal which generally causes decrease or increase in the normalized transmittance with the change in position with respect to focus [32]. For the measurement of transmittance in open aperture, the crystal was fixed on sample holder and kept at focus. After placing sample at focus, the sample holder was moved towards and far away from the source ($-z$ to $+z$) and corresponding transmittance was measured using detector. It was observed that normalized transmittance reduces, which results in a valley at the focus and is shown in figure 14.

This observation clearly signifies that the crystal is having revere saturation absorption behaviour (RSA) and should have positive β-value. The positive value of β is an important aspect of material characteristics, which tells that

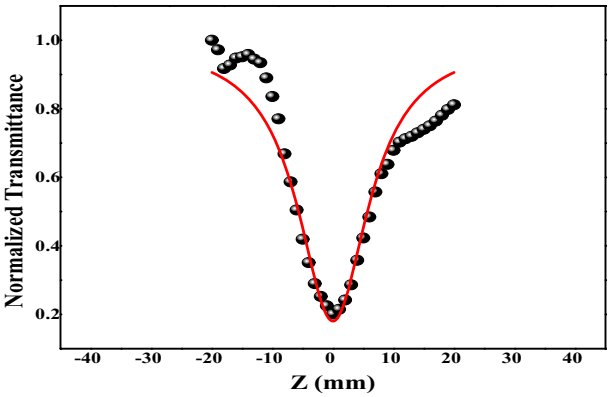

Figure 14. Open aperture Z-scan.

crystals may be useful in optical limiter. The value of β is calculated by the fitting of experimental data with the following equation [33]:

$$T(z) = 1 - \frac{\beta I_0 L_{\text{eff}}}{2^{3/2}\left(1 + \left[\frac{Z}{Z_0}\right]^2\right)} \tag{15}$$

Here L_{eff} is known as the effective thickness of used crystal and is given by

$$L_{\text{eff}} = \frac{1 - e^{-\alpha L}}{\alpha} \tag{16}$$

Here α is known as linear absorption coefficient, which has been calculated from UV–Visible spectroscopy data corresponding to wavelength of 800 nm. $Z_0 = \pi\omega_0^2/\lambda$ is known as the Rayleigh range for the laser beam with beam waist ω_0. The ω_0 can be calculated using $\omega_0 = 1.27f\lambda/2d$, which is found to be 40.64 μm, where d is the beam diameter. The value of NLA coefficient (β) was also evaluated by the use of experimental data using in the relation

$$\beta = \frac{2^{3/2}\Delta T}{I_0 L_{\text{eff}}} \tag{17}$$

The value of β was evaluated to be 4.25×10^{-12} cm W^{-1} and the fitted data shows that crystal exhibits the two photon absorption (2PA) phenomena; a vital parameter for optical limiting applications. The closed aperture Z-scan has been performed to measure NLR index of the material. It has been done by placing an aperture of radius (r_a) 0.5 mm in between the source and sample.

Figure 15 shows the valley to peak form, in which variation of normalized transmittance (T) with position is given, which signifies that NLR index (n_2) of titled crystal is positive and is self-focusing in nature. The change of normalized transmittance for closed aperture between peak to valley (ΔT_{P-V}) can be given by the relation

$$\Delta T_{P-V} = 0.496(1 - S)^{1/4}|\Delta\Phi| \tag{18}$$

Here S being the aperture linear transmittance is a function r_a and beam radius at aperture (ω_a) and is determined

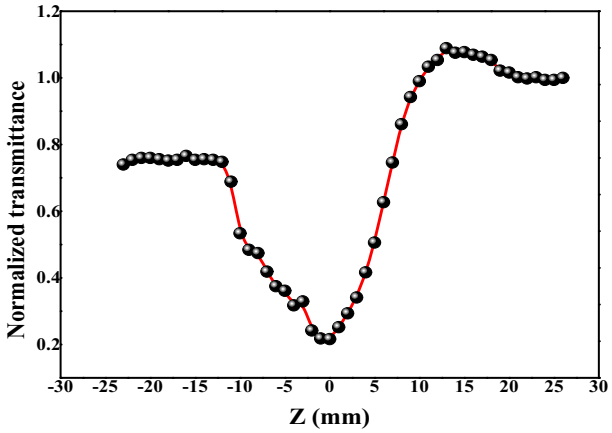

Figure 15. Closed aperture Z-scan.

using the following equation:

$$s = 1 - e^{\left[\frac{-2r_a^2}{\omega_a^2}\right]} \tag{19}$$

The value of n_2 could be evaluated using nonlinear phase shift ($\Delta\Phi$), which has been calculated from the experimental data by the use of given equation

$$n_2 = \frac{\lambda_L \Delta\Phi}{2\pi I_0 L_{\text{eff}}} \tag{20}$$

The value of NLR index was figured out to be 2.19×10^{-17} cm^2 W^{-1}. The coupling factor (ρ') is derived using the relation

$$\rho' = \frac{\lambda_L \beta \times 10^2}{4\pi n_2} \tag{21}$$

The value of ρ' was found to be 123.5, which suggests that nonlinear absorbance is more dominance than nonlinear refraction for this single crystal. Hence open aperture and closed aperture studies of the IMDA single crystal suggest that it can be an appropriate material for self-focusing and optical limiting applications.

4. Conclusions

A transparent bulk size IMDA single crystal was harvested by SEST in a controlled environment. The existence of strain in the crystal was measured from the PXRD data using Hall–Willamson relation. Third-order nonlinearity of solution harvested IMDA single crystal has been studied by Z-scan technique. The physical parameters NLR index and NLA coefficient were calculated to be 2.19×10^{-17} cm^2 W^{-1} and 4.25×10^{-12} cm W^{-1}, respectively. The self-focusing nature of IMDA was obtained from closed aperture and the 2PA behaviour of the same sample was obtained from open aperture Z-scan accordingly. The DC obtained from HRXRD indicates that ingot possess interstitial-type defects. The optical transmittance of the grown material and low dielectric loss at higher frequencies region suggests that it is transparent for entire visible region with good optical quality. The higher value of stiffness constant grown crystal has good mechanical strength, which is a useful property in finding the applicability of the material. Hence it can be concluded that the grown crystal can be suitable for various optoelectronics and NLO applications.

Acknowledgements

We are thankful to Director CSIR-NPL, New Delhi, for encouragement for different characterization. Debabrata Nayak is gratefully thankful to University Grants Commission (UGC) for the financial support and AcSIR-NPL for Ph.D. registration.

References

[1] Siva Bala Solanki S, Rajesh N P and Suthan T 2017 *Opt. Laser Technol.* **93** 143
[2] Vijayan N, Rani N, Madhurambal G, Bhagavannarayana G, Rathi B, Philip R *et al* 2013 *J. Therm. Anal. Calorim.* **112** 1113
[3] Preeti Singh, Mohd. Hasmuddin, Mohd. Shakir, Vijayan N, Abdullah M M, Ganesh V *et al* 2013 *Mater. Chem. Phys.* **142** 154
[4] Karuppasamy P, Muthu Senthil Pandian, Ramasamy P and Sunil V 2018 *Opt. Mater.* **79** 152
[5] Tomita Y, Ando T and Ueno K 1965 *Bull. Chem. Soc. Jpn.* **38** 138
[6] Parameswari A, Shamima Hussain, Premkumar R, Mohamed Asath R and Milton Franklin Benial A 2018 *Analyt. Chem. Lett.* **8** 437
[7] Sonia, Vijayan N, Medha Bhushan, Kanika Thukral, Rishabh Raj, Maurya K K *et al* 2017 *J. Appl. Cryst.* **50** 763
[8] Batterman B W and Cole H 1964 *Rev. Mod. Phys.* **36** 681
[9] Bhuvana K Periyasamy, Robinson S Jebas, Gopalakrishnan N and Balasubramanian T 2007 *Mater. Lett.* **61** 4246
[10] Narayan Bhat M and Dharmaprakash S M 2002 *J. Cryst. Growth* **236** 376
[11] Koteeswari P, Suresh S and Mani P 2012 *J. Miner. Mater. Char. Eng.* **11** 813
[12] Tauc J 1968 *Mater. Res. Bull.* **3** 37
[13] Manikandan S, Sabari Girisun T C, Mohandoss R, Dhanuskodi S and Manivannan S 2014 *Opt. Spectrosc.* **117** 469
[14] Krishna Kumar M, Sudhahar S, Pandi P, Bhagavannarayana G and Mohan Kumar R 2014 *Opt. Mater.* **36** 988
[15] Arora S K, Kothari A, Amin B and Chudasama B 2007 *Cryst. Res. Technol.* **42** 589
[16] Sangwal K 2000 *Mater. Chem. Phys.* **63** 145
[17] Sonia, Vijayan N, Mahak Vij, Anuj Krishna, Harsh Yadav, Maurya K K *et al* 2019 *Appl. Phys. A* **125** 363
[18] Hays C and Kendall E G 1973 *Metallography* **6** 275
[19] Riscob B, Shkir Mohd, Ganesh V, Vijayan N, Maurya K K, Kishan Rao K *et al* 2014 *J. Alloys Compd.* **588** 242
[20] Susmita Karan and Sen Gupta S P 2005 *Mater. Sci. Eng. A* **398** 198

[21] Gayathri K, Krishnan P, Rajkumar P R and Anbalagan G 2014 *Bull. Mater. Sci.* **37** 1589
[22] Philip J and Prasada Rao T A 1992 *Phys. Rev. A* **46** 2163
[23] Coles H J and Kershaw S V 1988 *J. Chem. Soc. Faraday* **84** 987
[24] Lin H M, Chen Y F, Shen J L and Chou W C 2001 *J. Appl. Cryst.* **89** 4476
[25] Shan-Shan Yu, Guo-Jun Yuan and Hai-Bao Duan 2015 *RSC Adv.* **5** 45213
[26] Madhangi M, Jauhar RO MU and Murugakoothan P 2019 *AIP Conf. Proc.* **2115** 030403
[27] Suresh S and Arivuoli D 2011 *J. Miner. Mater. Char. Eng.* **10** 1131
[28] Suresh S and Arivuoli D 2011 *J. Optoelectron. Biomed. Mater.* **3** 63
[29] Ravindra N M and Srivastava V K 1980 *Infrared Phys.* **20** 67
[30] Penn D R 1962 *Phys. Rev.* **128** 2093
[31] Eric W Van Stryland, Kuzyk M G and Dirk C W 1998 *Characterization techniques and tabulations for organic nonlinear materials* (New York: Marcel Dekker, Inc.) p 655
[32] Arivazhagan T, Siva Bala Solanki S and Narayana Perumal Rajesh 2017 *Opt. Laser Technol.* **88** 188
[33] Zidan M D, Al-Ktaifani M and Allahham A 2015 *Opt. Laser Technol.* **70** 45